

# The Hartree ensemble approximation revisited: The “symmetric phase”

Mischa Sallé\* and Jan Smit†

*Institute for Theoretical Physics, University of Amsterdam  
Valckenierstraat 65, 1018 XE Amsterdam, the Netherlands*

(Dated: October 28, 2018)

The Hartree ensemble approximation is studied in the “symmetric phase” of 1+1 dimensional  $\lambda\phi^4$  theory. In comparison with the “broken phase” studied previously, it is shown that the dynamical evolution of observables such as the particle distribution, energy exchange and auto-correlation functions, is substantially slower. Approximate thermalization is found only for relatively large energy densities and couplings.

PACS numbers: 11.10.Wx, 05.70.Ln, 11.15.Ha

## I. INTRODUCTION

Non-perturbative treatments of relativistic quantum fields out of equilibrium are currently under intense investigation, because of their importance in applications to the physics of the early universe and to heavy-ion collisions. The Hartree approximation is sufficiently simple that it facilitates the study of inhomogeneous systems by numerical methods. The possibility of inhomogeneity allows for the incorporation of non-perturbative configurations such as sphalerons and Skyrmions, or kinks in 1+1 dimensions.

Another aspect of inhomogeneity relates to equilibration and thermalization. For homogeneous systems, the usual Hartree approximation fails to describe thermalization, because it does not incorporate direct scattering. On the other hand, the classical approximation, in which expectation values are obtained as an average over realizations which are specified by an initial distribution, does allow for (classical) thermalization [1]. The reason is that the realizations are typically inhomogeneous, even if the initial distribution is homogeneous, which allows for scattering of the classical waves. (Clearly, strictly homogeneous classical scalar-field configurations cannot thermalize as these correspond to a dynamical system with only one degree of freedom.) Classical waves that are small fluctuations on a ground state, correspond in the quantum analogue to a homogeneous mean field with a relatively small (“vacuum size”) two-point function. The classical scattering of such waves would correspond to direct scattering in the quantum analogue, which is absent in the Hartree approximation. However, one may doubt, if strongly non-linear classical waves can be very well represented, in their quantum analogue, by two-point functions with, necessarily approximate, direct-scattering terms in their evolution equations. One can furthermore imagine that in such situations strong non-

linearity is important for the first stages of equilibration, and that this aspect could be better represented by strong and typically inhomogeneous mean fields.

Motivated by the capability of the classical description to incorporate strong non-linearity, we recently introduced [2, 3] a Hartree-ensemble approximation, in which the initial density matrix is expanded on a basis of Gaussian coherent states,

$$\hat{\rho} = \int D\phi D\pi \rho[\phi, \pi] |\phi\pi\rangle\langle\phi\pi|, \quad (1)$$

with “mean fields”  $\phi$  and  $\pi = \dot{\phi}$  and suitable variances. With “mean field” we here denote the expectation value in the Gaussian quantum density matrix  $|\phi, \pi\rangle\langle\phi, \pi|$ . The true mean fields are obtained after taking also the classical average over the separate “realizations”, weighted with the classical density functional  $\rho[\phi, \pi]$ . For each of these “realizations” separately we use the Hartree approximation.

This formulation achieves two things. First, it allows for the description of systems with non-Gaussian initial density matrices, thereby going beyond the Hartree approximation, and second, it allows for strongly non-linear equilibration. There is also a remnant of the “small fluctuation type” scattering: the “mean fields” in the “realizations”  $|\phi\pi\rangle\langle\phi\pi|$  are in general inhomogeneous, even if the full expectation values describe a homogeneous system, and these inhomogeneities lead to indirect scattering of the quantum modes via the Fourier modes of the inhomogeneous “mean field”.<sup>1</sup>

Note that when the initial distribution  $\rho[\phi, \pi]$  is positive, the initial correlation functions can in principle be calculated to arbitrary precision using Monte Carlo methods. However, the dynamical equations of motion still apply to an individual Gaussian “realization”, using a Gaussian approximation (Hartree), and the correlation functions at later times depend on these approximations. When the “mean field” dynamics in the “re-

---

\*Electronic address: mischa.salle@helsinki.fi; current address: Helsinki Institute of Physics, P.O. Box 64, FIN-00014 University of Helsinki, Finland

†Electronic address: jsmit@science.uva.nl

---

<sup>1</sup> Of course, we would like to include direct scattering as well, as in [4], but this is at present numerically too demanding in the inhomogeneous case.

alizations” dominates over the Hartree corrections, we expect that this Hartree-ensemble method works better than the usual Hartree method in terms of the true mean field, especially in case the latter is homogeneous.

In Ref. [2, 3] we studied this extension of the usual Hartree approximation in the 1+1 dimensional  $\phi^4$  model, and found that it leads to approximate thermalization. We focused on the “broken phase” of the system in these papers. In the present work we discuss the “symmetric phase”.<sup>2</sup>

The reason for presenting results also in the “symmetric phase” is twofold. First, it is interesting in its own right. Not much is known yet about inhomogeneous relativistic systems out of equilibrium and numerical data can help to sharpen our intuition. Second, results by Betencourt et al. [5], which were obtained in the “symmetric phase”, appear to contradict our earlier results in [2, 3]. We try to clarify the situation here, and substantiate our earlier observation that the evolution towards equilibrium in the “symmetric phase” is much slower than in the “broken phase”.

Broadly speaking, our results are as follows. We find (relatively) rapid approximate thermalization from an initial homogeneous non-equilibrium density matrix, in case of *high* energy-densities. We interpret this as concurring our intuition on strong “mean fields”. On the other hand, for *low* energy densities and/or couplings the time scales for reasonable changes in particle distribution functions are huge, even larger than what we found earlier in the “broken phase”, which makes numerical study very difficult. The inhomogeneous case studied by Betencourt et al. [5] (a single Gaussian wave packet) falls in the low energy density class and indeed, even after very large times, we do not find thermalization. A more complete summary of the many detailed results will be given at the end of this paper.

In Sec. II we will briefly review the equations of motion, explain the Hartree ensemble approximation, describe various initial conditions and observables, and describe some aspects of the elegant definition of the theory on a space-time lattice. In Sec. III we will present results obtained using numerical simulations. We give an explanation of a phenomenon found in the simulations that we call “local  $k$ -space equilibration” in Sec. IV, where we also comment on the difference between the “symmetric” and “broken phase”. A discussion is in Sec. V. Finally in the Appendix we derive the initial as well as free-field form of the particle distribution for the Gaussian wave packet.

In the rest of this paper we will drop the quotes around

“mean field”.

## II. HARTREE APPROXIMATIONS, INITIAL CONDITIONS AND OBSERVABLES

### A. Hartree approximation

For the  $\lambda\phi^4$  theory in 1+1 dimensions the Heisenberg equations of motion are given by

$$(-\partial^2 + \mu^2)\hat{\phi}(x) + \lambda\hat{\phi}(x)^3 = 0. \quad (2)$$

In the Hartree approximation (H.a.) we can write  $\hat{\phi}(x)$  and its time derivative  $\hat{\pi}(x)$  as

$$\hat{\phi}(x) \stackrel{\text{H.a.}}{=} \phi(x) + \sum_{\alpha} \left[ \hat{b}_{\alpha}^{\dagger} f_{\alpha}(x) + \hat{b}_{\alpha} f_{\alpha}^{*}(x) \right], \quad (3a)$$

$$\hat{\pi}(x) \stackrel{\text{H.a.}}{=} \pi(x) + \sum_{\alpha} \left[ \hat{b}_{\alpha}^{\dagger} \dot{f}_{\alpha}(x) + \hat{b}_{\alpha} \dot{f}_{\alpha}^{*}(x) \right], \quad (3b)$$

where  $\phi(x) = \langle \hat{\phi}(x) \rangle$  and  $f_{\alpha}(x)$  are the time-dependent mean field and mode functions, and  $\hat{b}_{\alpha}$  are time-independent creation and annihilation operators satisfying the usual commutation relations. Without an approximation a similar expansion is possible but only with time-dependent creation and annihilation operators: in terms of the initial  $\hat{b}_{\alpha}$  and  $\hat{b}_{\alpha}^{\dagger}$  the dependence is then non-linear at later times. The fact that the same set can be used at all times is due to the Gaussianity of the Hartree approximation (see e.g. [2] for more information). Combining Eqs. (3) and (2) and taking expectation values gives the equations of motion for  $\phi$  and the  $f_{\alpha}$ ,

$$\ddot{\phi} = \Delta\phi - [\mu^2 + \lambda\phi^2 + 3\lambda C]\phi, \quad (4a)$$

$$\ddot{f}_{\alpha} = \Delta f_{\alpha} - [\mu^2 + 3\lambda\phi^2 + 3\lambda C]f_{\alpha}, \quad (4b)$$

with

$$C = \sum_{\alpha} (2n_{\alpha}^0 + 1)|f_{\alpha}|^2, \quad n_{\alpha}^0 = \langle \hat{b}_{\alpha}^{\dagger} \hat{b}_{\alpha} \rangle. \quad (4c)$$

The exact equation of motion for the one-point function, which follows by taking the expectation value of the Heisenberg equation of motion (2), contains the three-point function. An exact equation for the three-point function can be obtained from taking the expectation value of the product of Eq. (2) with two field operators and will contain the five-point function. The resulting infinite hierarchy of higher point functions is truncated by the Hartree approximation which factorizes these higher-point functions into one- and two-point functions.

### B. Choice of mode functions and renormalization

As in our previous work, we will use the stationary solutions of Eqs. (4) to define the initial mode functions,

<sup>2</sup> At zero temperature the expectation value of the order field  $\phi$  distinguishes the phase regions in coupling-parameter space. At finite temperature this expectation value vanishes due to kink-antikink condensation. However, there is still a clear distinction in the behaviour of the system in the two phases even in finite volume.

i.e. we will choose them as plane waves with wave vector  $k$  ( $\alpha \rightarrow k$ )

$$f_k(x, 0) = \frac{e^{ikx}}{\sqrt{2\omega_k^{(0)}L}}, \quad \dot{f}_k(x, 0) = -i\omega_k^{(0)} \frac{e^{ikx}}{\sqrt{2\omega_k^{(0)}L}}. \quad (5)$$

Here  $L$  is the ‘‘volume’’ of our one dimensional system (using periodic boundary conditions) and  $\omega_k^{(0)} = \sqrt{m^2 + k^2}$ , with  $m$  the physical mass, defined self-consistently as the square root of the term in square brackets in Eq. (4b). The sum (4c) for these initial mode functions diverges logarithmically in 1+1 D, which is compensated by the bare  $\mu^2$ . In the vacuum, i.e. using stationary solutions for  $\phi$  and  $f_\alpha$  of Eqs. (4) with  $n_\alpha^0 = 0$ , the renormalized mass parameter and mode sum are given by

$$\mu_{\text{ren}}^2 = \mu^2 + 3\lambda C_{n_\alpha^0=0}, \quad \mu^2 + 3\lambda C = \mu_{\text{ren}}^2 + 3\lambda C_{\text{ren}}. \quad (6)$$

Then  $m^2 = \mu_{\text{ren}}^2 + 3\lambda v^2$ , with  $v$  the stationary value of  $\phi$ .

In this paper we will use  $n_\alpha^0 = 0$ . Using the mode functions (5), the coherent states  $|\phi, \pi\rangle$  satisfying  $b_k|\phi, \pi\rangle = 0$ , have mean fields  $\phi(x)$  and  $\pi(x)$ , with a variance that is easily computed. We shall use these states as basis for our Hartree ensembles (1).

### C. Initial conditions

We used two different initial conditions for the mean field, a sum of standing waves with a flat distribution of phases, which we also used in our previous work in the ‘‘broken phase’’ [2], and a single Gaussian wave packet, as studied by Bettencourt et al. [5].

The first is given by

$$\phi(x) = 0, \quad \pi(x) = Am \sum_{j=1}^{j_{\text{max}}} \cos(2\pi jx/L - \psi_j), \quad (7)$$

where the maximum momentum  $2\pi j_{\text{max}}/L$  is typically of the order of the mass  $m$  and the constants  $\psi_j$  are random phases with a flat distribution (i.e. they are uniformly distributed in  $[0, 2\pi)$ ). We shall call such  $\rho[\phi, \pi]$  flat ensembles. The energy, which is independent of the phases  $\psi_j$ , is given by

$$\frac{E}{m} = \frac{A^2 L m j_{\text{max}}}{4}. \quad (8)$$

We use both  $A$  and  $j_{\text{max}}$  to vary the total energy density.

The second initial condition is a Gaussian wave packet:

$$\pi(x) = 0, \quad \phi(x) = \Phi \exp\left[-\frac{x^2}{2A}\right]. \quad (9)$$

Its energy is given by

$$\frac{E}{m} = \frac{\Phi^2}{8} \sqrt{\frac{\pi}{Am^2}} (2 + 4Am^2 + \sqrt{2}A\lambda\Phi^2). \quad (10)$$

We will restrict ourselves to  $Am^2 = 2$  and use  $\Phi$  to vary the total energy in the system. For this type of initial conditions we do not average over multiple runs, so  $\rho[\phi, \pi]$  is a delta functional and  $\hat{\rho}$  is a coherent pure state.

### D. Observables

As in [2] we define particle numbers  $n_k$  and frequencies  $\omega_k$  in terms of equal time correlation functions,

$$S(x, y) = \overline{\langle \hat{\phi}(x) \hat{\phi}(y) \rangle} - \overline{\langle \hat{\phi}(x) \rangle} \overline{\langle \hat{\phi}(y) \rangle}, \quad (11a)$$

$$U(x, y) = \overline{\langle \hat{\pi}(x) \hat{\pi}(y) \rangle} - \overline{\langle \hat{\pi}(x) \rangle} \overline{\langle \hat{\pi}(y) \rangle}. \quad (11b)$$

The over-line indicates coarse graining over all space and, depending on the simulation, also includes course graining over a time interval and an ensemble of initial conditions. The symmetrized  $\pi\phi$ -correlation function,  $T(x, y)$ , vanishes in equilibrium, and we will just use  $S$  and  $U$ . Taking the average over all of space leaves  $S$  and  $U$  depending only on the coordinate difference  $x - y$ . In terms of the Fourier transform,

$$S_k = \int dx e^{-ikx} S(x, 0) \quad (12)$$

and similar for  $U$ , the time-dependent particle numbers and frequencies are defined by

$$S_k = \left(n_k + \frac{1}{2}\right) \frac{1}{\omega_k}, \quad U_k = \left(n_k + \frac{1}{2}\right) \omega_k. \quad (13)$$

Therefore, apart from numerical corrections discussed in Sec. II E, we define instantaneous particle number and frequency by

$$n_k = \sqrt{U_k S_k} - \frac{1}{2}, \quad \omega_k = \sqrt{\frac{U_k}{S_k}}. \quad (14)$$

In practice  $n_k$  is positive (it can be shown to be positive provided the symmetric correlation between  $\phi$  and  $\pi$  vanishes). Other definitions of particle numbers are in use, e.g. derived from time-dependent creation and annihilation operators defined in terms of adiabatic mode functions,

$$\hat{a}_k(t) e^{-i \int_0^t dt' \tilde{\omega}_k(t')} = \frac{1}{\sqrt{2\tilde{\omega}_k(t)L}} \int_0^L dx e^{-ikx} [\tilde{\omega}_k(t) \hat{\phi}(t, x) + i\hat{\pi}(t, x)]. \quad (15)$$

However, one then still has to choose  $\tilde{\omega}_k(t)$ . This can introduce some ambiguity, especially if the system is far from equilibrium and the effective mass term in the equations of motion for the modes becomes negative; see for example [6, 7]. Using Eq. (14) as the definition of particle number, has the advantage that the frequencies are real and positive by construction.

The correlation functions  $S$  and  $U$  may be written as a sum of contributions from the mean field and mode

functions separately. Given  $\omega_k$  as obtained from the total  $S$  and  $U$ , we can study their separate contributions to  $n_k$  as defined by Eqs. (13).

The energy density can be obtained from the effective Hamiltonian  $H_{\text{eff}} = \langle \hat{H} \rangle$  [2]. We split it into mean field and mode contributions according to

$$E_{\text{mf}} = \frac{1}{2}(\partial_t \phi)^2 + \frac{1}{2}(\partial_x \phi)^2 + \frac{1}{2}\mu_{\text{ren}}^2 \phi^2 + \frac{1}{4}\lambda \phi^4 - \frac{1}{2}\mu_{\text{ren}}^2 v^2 - \frac{1}{4}\lambda v^4, \quad (16a)$$

$$E_{\text{modes}} = \sum_{\alpha} \left( \frac{1}{2} + n_{\alpha}^0 \right) (|\partial_t f_{\alpha}|^2 + |\partial_x f_{\alpha}|^2) + \frac{1}{2}\mu_{\text{ren}}^2 C_{\text{ren}} + \frac{3}{2}\lambda C_{\text{ren}} \phi^2 + \frac{3}{4}\lambda C_{\text{ren}}^2 - H_{\text{vac}} \quad (16b)$$

where  $v$ , the ground-state value of  $\phi$ , is zero in the ‘‘symmetric phase’’. Although the splitting between modes and mean field is somewhat arbitrary, the above definition has the advantage that it reduces to the classical expression when the modes are of the vacuum form (5).

The quasi-particle energy is also an interesting observable. It may be defined as

$$E_{\text{qp}} = \sum_k n_k \omega_k \quad (17)$$

where  $n_k$  can be obtained from the two-point functions of the mean field, of the mode functions, or of the sum of both.

### E. Implementation on a lattice

The discretization of the scalar field theory on a space-time lattice has some elegant features which we present briefly in this section; for fermions, see [8]. For simplicity we start with a simple quantum mechanical system of unit mass, with action

$$S = a_0 \sum_t \left\{ \frac{[q(t+a_0) - q(t)]^2}{2a_0^2} - V(q(t)) \right\}, \quad (18)$$

where  $a_0$  is the time step,  $t = a_0 r$ , with integer  $r$ . We define the quantum system by means of the path integral. The discretized path integral

$$Z = \int \left[ \prod_t dq(t) \right] e^{iS} \quad (19)$$

corresponds to an evolution operator in Hilbert space that is a product of single step evolution operators given by

$$\hat{U} = \hat{U}_p \hat{U}_q, \quad (20)$$

with

$$\hat{U}_p = e^{-ia_0 \hat{p}^2/2}, \quad \hat{U}_q = e^{-ia_0 V(\hat{q})}, \quad (21)$$

where  $\hat{p}$  and  $\hat{q}$  are canonical operators satisfying  $[\hat{q}, \hat{p}] = i$ . A finite time evolution then takes the ‘‘Trotter form’’

$$\hat{U}_q \hat{U}^r = \hat{U}_q \cdots \hat{U}_p \hat{U}_q \hat{U}_p \hat{U}_q \hat{U}_p \hat{U}_q \cdots \hat{U}_q, \quad (22)$$

The Heisenberg operators

$$\hat{p}(t) = \hat{U}^{r\dagger} \hat{p} \hat{U}^r, \quad \hat{q}(t) = \hat{U}^{r\dagger} \hat{q} \hat{U}^r, \quad t = a_0 r, \quad (23)$$

satisfy the discretized equations of motion in leapfrog fashion,

$$\hat{p}(t+a_0) = \hat{p}(t) - a_0 V'(\hat{q}(t)), \quad (24a)$$

$$\hat{q}(t+a_0) = \hat{q}(t) + a_0 \hat{p}(t+a_0). \quad (24b)$$

With  $\hat{q}(t) \rightarrow q(t)$ ,  $\hat{p}(t) \rightarrow [q(t) - q(t-a_0)]/a_0$ , the above Eqs. (24) are identical in form to the classical equations obtained from the stationary action principle.

Making a unitary transformation

$$\hat{T} = e^{-ia_0 V(\hat{q})/2} \hat{U} e^{ia_0 V(\hat{q})/2}, \quad (25)$$

we get an equivalent operator  $\hat{T}$ , which becomes the Hermitian and positive transfer operator upon analytically continuing to imaginary time (see e.g. [9]), writing  $a_0 = e^{-i\theta} |a_0|$ ,  $\theta = 0 \rightarrow \pi/2$ ,

$$\hat{T} \rightarrow e^{-|a_0|V(\hat{q})/2} e^{-|a_0|\hat{p}^2/2} e^{-|a_0|V(\hat{q})/2}. \quad (26)$$

Specializing to the harmonic case  $V(q) = \omega^2 q^2/2$  we can diagonalize the time evolution in terms of creation and annihilation operators  $\hat{c}^\dagger$  and  $\hat{c}$ ,

$$\hat{T} \hat{c} \hat{T}^\dagger = e^{ia_0 \omega^{(e)}} \hat{c}, \quad \hat{T} \hat{c}^\dagger \hat{T}^\dagger = e^{-ia_0 \omega^{(e)}} \hat{c}^\dagger, \quad (27)$$

with

$$\hat{c} = \frac{1}{\sqrt{2\omega^{(n)}}} (\omega^{(n)} \hat{q} + i\hat{p}) \quad (28)$$

and

$$\cos(a_0 \omega^{(e)}) = 1 - \frac{1}{2} a_0^2 \omega^2, \quad (29a)$$

$$\omega^{(n)} = \frac{1}{a_0} \sin(a_0 \omega^{(e)}) = \omega \sqrt{1 - \frac{1}{4} a_0^2 \omega^2}, \quad (29b)$$

and the conjugate relation for  $\hat{c}^\dagger$ . The creation and annihilation operators satisfy the standard commutation relation  $[\hat{c}, \hat{c}^\dagger] = 1$ . The superscripts  $e$  and  $n$  distinguish the ‘‘exponent omega’’ (eigenvalue omega)  $\omega^{(e)}$  from the ‘‘normalization omega’’ (eigenvector omega)  $\omega^{(n)}$ , and both go over to the ‘‘original omega’’  $\omega$  in the continuous time limit  $a_0 \rightarrow 0$ . The ground state is given by

$$\hat{c}|0\rangle = 0, \quad \langle q|0\rangle = \nu e^{-\omega^{(n)} q^2/2}, \quad (30)$$

with  $\nu$  a normalization constant and

$$\hat{T} (\hat{c}^\dagger)^n |0\rangle = e^{-i(n+1/2)a_0 \omega^{(e)}} (\hat{c}^\dagger)^n |0\rangle. \quad (31)$$

The evolution becomes unstable when  $a_0^2\omega^2 > 4$ , for which  $\omega_k^{(e)}$  is imaginary. The eigenvalues of  $\hat{T}$  are then no longer phase factors and its eigenfunctions no longer normalizable, despite its formally unitary form. This is of course avoided by taking  $a_0$  sufficiently small. The discretization errors in  $\omega^{(e)}$  and  $\omega^{(n)}$  are of order  $a_0^2$ .

It is natural to identify the Hamiltonian  $\hat{H}$  from  $\hat{T} = \exp(-ia_0\hat{H})$ , but this leaves a modulo  $2\pi/a_0$  ambiguity for the eigenvalues of  $\hat{H}$  (the imaginary time version is unambiguous). To pin down  $\hat{H}$  more precisely we can use the Baker-Campbell-Hausdorff series for combining the exponents in  $\hat{T}$ , which gives  $\hat{H} = \hat{p}^2/2 + V(\hat{q}) + \mathcal{O}(a_0^2)$ . We shall neglect the corrections of order  $a_0^2$ . The exact  $\hat{H}$  is time independent. In practice, the expectation value of the approximate  $\hat{H}$  is constant in time up to small fluctuations, as expected for a leapfrog algorithm.

For application to the Hartree approximation it will be more convenient for us to work with the unitarily related creation and annihilation operators that diagonalize  $\hat{U}$ ,

$$\begin{aligned} \hat{a} &= e^{ia_0V(\hat{q})/2} \hat{c} e^{-ia_0V(\hat{q})/2} \\ &= \frac{1}{\sqrt{2\omega^{(n)}}} \left( \frac{1 - e^{-ia_0\omega^{(e)}}}{ia_0} \hat{q} + i\hat{p} \right), \end{aligned} \quad (32)$$

$$\hat{U}\hat{a}\hat{U}^\dagger = e^{ia_0\omega^{(e)}} \hat{a}, \quad (33)$$

for  $V = \omega^2 q^2/2$ . Note that  $\hat{a} \rightarrow \hat{c}$  in the limit  $a_0 \rightarrow 0$ .

The generalization of the above quantum mechanical model to our scalar field is straightforward. The lattice action on a space-time lattice with spatial-temporal lattice distance  $a/a_0$  is given by

$$\begin{aligned} S[\phi] &= a_0 a \sum_{x,t} \left\{ \frac{[\phi(x,t+a_0) - \phi(x,t)]^2}{2a_0^2} \right. \\ &\quad - \frac{[\phi(x+a,t) - \phi(x,t)]^2}{2a^2} - \frac{1}{2} \mu^2 \phi(x,t)^2 \\ &\quad \left. - \frac{1}{4} \lambda \phi(x,t)^4 \right\}, \end{aligned} \quad (34)$$

where we assume a periodic physical size  $L = Na$ . The operator description in Hilbert space follows from the lattice regularized path integral. In the Hartree approximation we write the operator fields in terms of a complete set of mode functions,

$$\hat{\phi}(x,t) = \phi(x,t) + \sum_k [\hat{b}_k f_k(x,t) + \hat{b}_k^\dagger f_k(x,t)^*], \quad (35a)$$

$$\hat{\pi}(x,t) = \pi(x,t) + \sum_k [\hat{b}_k \dot{f}_k(x,t) + \hat{b}_k^\dagger \dot{f}_k(x,t)^*], \quad (35b)$$

where the use of

$$\dot{f}(x,t) = \frac{f(x,t) - f(x,t-a_0)}{a_0} \quad (36)$$

is inspired by Eq. (24b). (Using instead the forward derivative  $\dot{f}_k(x,t) = [f(x,t+a_0) - f(x,t)]/a_0$  gives equivalent results.) Imposing canonical commutation relations

for both  $\hat{\phi}$ ,  $\hat{\pi}$  and  $\hat{b}_k$ ,  $\hat{b}_k^\dagger$ , leads to the orthonormality and completeness relations

$$a \sum_x [i\dot{f}_k(x,t) f_l^*(x,t) - i f_k(x,t) \dot{f}_l^*(x,t)] = \delta_{kl}, \quad (37a)$$

$$\sum_k [i f_k^*(x,t) \dot{f}_k(y,t) - i f_k(x,t) \dot{f}_k^*(y,t)] = \frac{\delta_{xy}}{a}. \quad (37b)$$

The time independence of the orthonormality conditions corresponds to Noether charges of symmetries [2] of the effective action on the lattice. We use the static solutions of the Hartree equations in constructing the set of mode functions. Their equation of motion

$$\begin{aligned} \frac{f_k(x,t+a_0) - 2f_k(x,t) + f_k(x,t-a_0)}{a_0^2} = \\ \frac{f_k(x+a,t) - 2f_k(x,t) + f_k(x-a,t)}{a^2} - m^2 f_k(x,t), \end{aligned} \quad (38)$$

can be written in the leapfrog form (24). The solution of the recursion relation (38) can be written as

$$f_k(x,t) = \frac{e^{ikx - i\omega_k^{(e)}t}}{\sqrt{2\omega_k^{(n)}L}}, \quad k = \frac{2\pi j}{L}, \quad j = -\frac{N}{2} + 1, \dots, \frac{N}{2}, \quad (39)$$

giving

$$-\frac{2 - 2\cos(\omega_k^{(e)}a_0)}{a_0^2} + \frac{2 - 2\cos(ka)}{a^2} + m^2 = 0. \quad (40)$$

Defining a lattice  $\omega_k^{(a)}$  as

$$\omega_k^{(a)} = \sqrt{m^2 + \frac{2 - 2\cos(ka)}{a^2}}, \quad (41)$$

we find the analogue of Eq. (29a),

$$\cos(a_0\omega_k^{(e)}) = 1 - \frac{1}{2} a_0^2 (\omega_k^{(a)})^2, \quad (42)$$

which has real  $\omega_k^{(e)}$  solutions for  $a/a_0 > \sqrt{4 + a^2 m^2}$ . We used  $a/a_0 = 10$  in our simulations, which amply secured stability. The normalization in Eq. (39) is fixed by the orthonormality relation (37a), which gives the analogue of Eq. (29b)

$$\omega_k^{(n)} = \frac{\sin(a_0\omega_k^{(e)})}{a_0} = \omega_k^{(a)} \sqrt{1 - \frac{1}{4} a_0^2 (\omega_k^{(a)})^2}, \quad (43)$$

The completeness relation (37b) is then also satisfied. When the mode functions have the form (39), the  $\hat{a}_k$  defined by  $\hat{\phi} = \sum_k \hat{a}_k f_k + \text{h.c.}$ ,  $\hat{\pi} = \sum_k \hat{a}_k \dot{f}_k + \text{h.c.}$ , are related to  $\hat{\phi}$  and  $\hat{\pi}$  as in the quantum mechanical case (32). Note that  $\omega_k^{(n)}, \omega_k^{(e)} \rightarrow \omega_k^{(a)}$  in the limit  $a_0 \rightarrow 0$ , and  $\omega_k^{(a)} \rightarrow \sqrt{m^2 + k^2}$  as  $a \rightarrow 0$ .

We end this section with a properly discretized version of the instantaneous particle number  $n_k$ , using the stationary solution (39) and the two-point functions (11). Suppose the mean field is zero and

$$\langle \hat{b}_k^\dagger \hat{b}_k \rangle = n_k^0 = n_{-k}^0. \quad (44)$$

Then

$$S_k(t) = \left( n_k^0 + \frac{1}{2} \right) \frac{1}{\omega_k^{(n)}}, \quad (45a)$$

$$U_k(t) = \left( n_k^0 + \frac{1}{2} \right) \frac{(\omega_k^{(a)})^2}{\omega_k^{(n)}}, \quad (45b)$$

where we used

$$\dot{f}_k(x, t) f_k^*(y, t) = (\omega_k^{(a)})^2 f_k(x, t) f_k^*(y, t). \quad (46)$$

Inverting Eqs. (45) we find that our definition of the instantaneous energy  $\omega_k(t)$  does not need discretization corrections,

$$\omega_k^{(a)} = \sqrt{\frac{U_k(t)}{S_k(t)}} \equiv \omega_k(t). \quad (47)$$

On the other hand, the definition of instantaneous particle number needs important corrections for large  $\omega_k$ :

$$n_k^0 + \frac{1}{2} = \sqrt{U_k S_k} \frac{\omega_k^{(n)}}{\omega_k^{(a)}} = \sqrt{U_k (S_k - \frac{1}{4} a_0^2 U_k)} \equiv n_k(t) + \frac{1}{2}, \quad (48)$$

using Eqs. (43) and (47).

For larger energies the corrections can become quite important. Denoting the uncorrected particle number by  $\tilde{n}_k = \sqrt{U_k S_k} - 1/2$ , we find

$$\begin{aligned} \frac{\tilde{n}_k - n_k}{n_k} &= \frac{n_k + \frac{1}{2}}{n_k} \left( \frac{1}{\sqrt{1 - \frac{1}{4} (a_0 \omega_k^{(a)})^2}} - 1 \right) \\ &\approx \frac{n_k + \frac{1}{2}}{n_k} \frac{1}{8} (a_0 \omega_k^{(a)})^2. \end{aligned} \quad (49)$$

Using a Bose-Einstein distribution at  $T = m$  and the typical value  $a_0 m = 1/80$  we find that the relative difference becomes unity for  $\omega_k/m = 7.5$ . At the lower temperature  $T/m = 0.5$  this is the case already for  $\omega_k/m = 4.3$ .

### III. NUMERICAL RESULTS

In this section we will present data we obtained using numerical simulations in the ‘‘symmetric phase’’, i.e.  $\mu^2$  and  $\lambda$  corresponding to the ‘‘symmetric phase’’ at zero temperature. First we will discuss the particle distribution to study its equilibration behaviour and to search for thermalization. Then we will examine the energies and auto-correlation function to analyse the time scales in the theory.

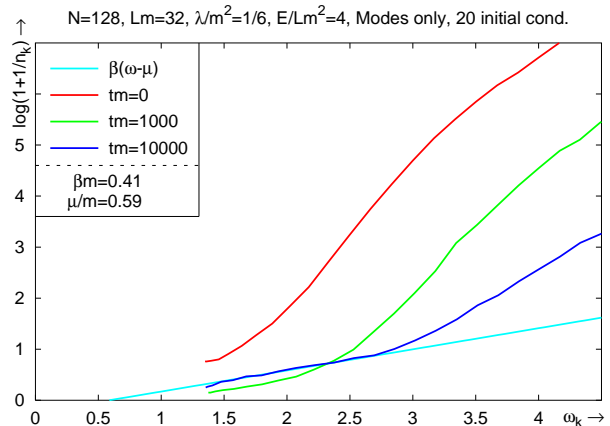


FIG. 1: The particle numbers  $\log(1 + 1/n_k)$  in the modes as a function of  $\omega_k$ . Average over 20 flat ensemble initial conditions,  $\lambda/m^2 = 1/6$ ,  $E/Lm^2 = 4$ , at times up to  $tm = 10^4$ . Time increases from the top curve to the bottom curve.

#### A. Flat ensemble

In the flat ensemble of initial conditions, the initial mean field  $\phi$  of a realization is equal to its vacuum expectation value 0, while its momentum is the sum of waves with random phase, as specified in Eqs. (7). We averaged over 10 or 20 initial conditions, and excited all non-zero modes up to  $k_{\max} = 2\pi j_{\max}/L = \pi m/2$ . Simulations have been carried out for three different couplings  $\lambda/m^2 = 1/6, 1/8, 1/12$  and three different energy densities  $E/Lm^2 = 4, 2, 1$ , as well as for the combination  $\lambda/m^2 = 0.1$  and  $E/Lm^2 = 0.4$ . We mainly used  $N = 128$  lattice points, and volume  $Lm = 32$ , while the temporal lattice distance  $a_0 = a/10$ .

##### 1. Particle distribution function

Fig. 1 shows the particle number obtained for coupling  $\lambda/m^2 = 1/6$  and energy density  $E/Lm^2 = 4$ . As in our previous work we compare the out-of-equilibrium particle densities with a Bose-Einstein (BE) distribution

$$n_k = \frac{1}{e^{(\omega_k - \mu)/T} - 1}. \quad (50)$$

We therefore plotted  $\log(1 + 1/n_k)$  versus  $\omega_k/m$ , since a BE distribution then shows up as a straight line with slope  $m/T$  and offset  $-\mu/m$  ( $T$  temperature,  $\mu$  chemical potential). For this largest coupling and energy density in our study we find approximate thermalization to the BE form with a temperature  $T/m = 2.4$  and chemical potential  $\mu/m = 0.6$ . In contrast to what was found in the ‘‘broken phase’’ [2, 3], a substantial chemical potential is needed to make a reasonable fit. Another difference is the larger time scale involved: in the ‘‘broken phase’’ at an energy density  $E/Lm^2 = 0.5$  and the same

	$E/Lm^2 = 1$	$E/Lm^2 = 2$	$E/Lm^2 = 4$
$\lambda/m^2 = 1/6$	$\beta m$ 1.12	0.71	0.41
	$\mu/m$ 0.95	0.83	0.59
$\lambda/m^2 = 1/8$	$\beta m$ 0.89*	0.60	0.45
	$\mu/m$ 0.62	0.76	0.80
$\lambda/m^2 = 1/12$	$\beta m$ --	0.68*	0.40
	$\mu/m$ --	0.76	0.85

TABLE I: Inverse temperature  $\beta$  and chemical potential  $\mu$  as derived from a Bose-Einstein fit to the particle numbers (modes only). See text for further explanation.

$\lambda/|\mu_{\text{ren}}^2| = 1/6$  ( $\lambda/m^2 = 1/12$ ), we could already recognize BE behaviour with  $T/m \approx 1$  at a time  $tm \lesssim 100$ , while here, at an 8 times larger energy and roughly 2 times larger effective BE temperature we can only clearly do so at time  $tm \gtrsim 2000$ . A fit of the local temperature  $T(t)$  approaching approximate equilibrium gives an equilibration-time scale  $m\tau_{\text{BE}} = 1500 - 1600$  (exponential fit over  $k/m < 1.7$ ,  $100 < t < 6000$ ).

For most parameters used in our simulations we can recognize Bose-Einstein features in the low momentum part of the distributions, and linear fits can be made as in Fig. 1. The results of these fits are shown in Table I. Fits marked with a star were made at  $tm = 59000 \dots 60000$ , all others at  $tm = 9000 \dots 10000$ . Including the mean field in the two-point functions, typically gives the same temperature within errors, but a noticeably larger value (+ 0.05) for  $\mu/m$ , corresponding to a higher particle number. The chemical potential is also more sensitive to the exact fit-interval than the temperature. In the two \*-marked runs a thermal distribution could be recognized only at times  $\gtrsim 20000$  ( $\lambda/m^2 = 1/12$ ) and  $\gtrsim 45000$  ( $\lambda/m^2 = 1/8$ ).

For the run at  $\lambda/m^2 = 1/12$ ,  $E/Lm^2 = 1$ , we did not find a thermal-like distribution even at the latest simulation time  $tm = 10^5$ . We see that the energy is transferred from the mean field to the modes and the system equilibrates “locally in  $k$ ”, but the total particle number remains roughly unchanged. The same was found at the lower energy density  $E/Lm^2 = 0.4$ , and also for the Gaussian wave packet initial condition. We interpret this as a resonance phenomenon in the equation of motion of the mode functions, which will be described in Section IV B.

Comparing the results at  $E/Lm^2 = 2$  and 4 it seems that the temperature only depends on the energy density and not on the coupling. This appears to hold even for the distribution function itself, as illustrated in Fig. 2, where the distributions for different couplings are plotted at different times. The different times at which the curves in the figure overlap suggest that the equilibration time scale for the particle distribution is proportional to  $\lambda^{-3}$ . The same power is found at the energy density  $E/Lm^2 = 2$ . Table I shows that the temperature is roughly proportional to  $\sqrt{E/L}$ , which can be understood from the scaling behaviour in Fig. 2, since there is

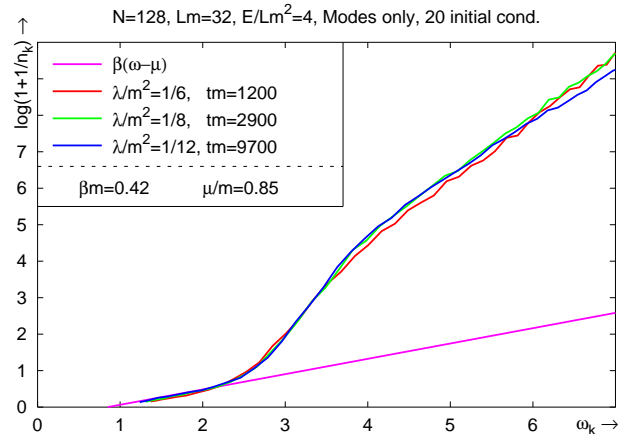


FIG. 2: Scaling behaviour of the particle distribution at fixed energy density and differing couplings and times.

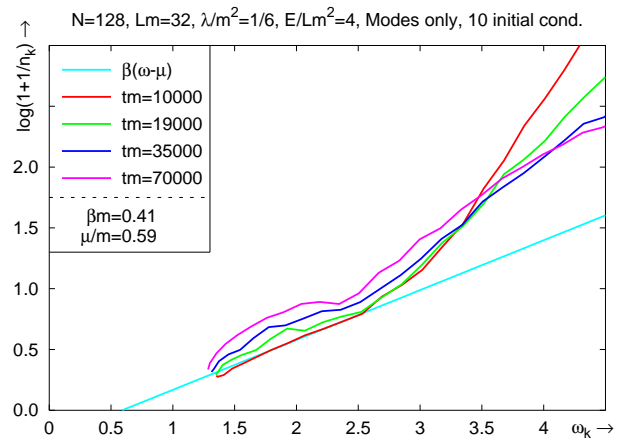


FIG. 3: The particle numbers  $\log(1+1/n_k)$  in the modes as a function of  $\omega_k$  at large times  $tm > 10^4$ . In the small  $k$  region time increases from bottom to top, in the large  $k$  region time increases from top to bottom.

no other scale left. The same argument should apply to the chemical potential. However, this quantity is more dependent on time than the temperature and runs at different parameters are best compared at different times as in Fig. 2, which we have not done in Table I.

The independence of coupling suggests that a representation of the energy in terms of almost free quasi-particles will be reasonably good. We will check this in the next section.

Fig. 3 shows the distribution for late times, when it starts to deviate from the BE form. Note the difference in vertical scale compared to Fig. 1. At  $tm = 15000 - 20000$  classical-like deviations become visible in the form of concave behaviour at low  $\omega_k$  ( $n_k = T/\omega_k \Rightarrow (\partial/\partial\omega_k)^2 \log(1+1/n_k) < 0$ ).

The mean field in this time region behaves very interestingly. In Fig. 4 we plotted the particle numbers at  $tm = 50000 \dots 70000$  as a function of momentum  $k$ , both

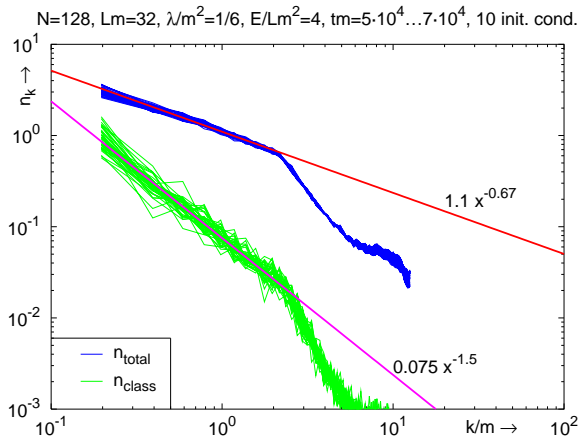


FIG. 4: Log-log plot of the particle numbers for mean field alone, and combined with modes, vs  $k/m$ , at large times.

for the mean field alone and for the total two-point function, using a log-log scale and leaving out the zero mode. While the high-momentum modes are still exponentially suppressed, the low-momentum modes have acquired a power law distribution. The quantum-modes-only distribution does *not* behave as a power law (cf. Fig. 3). The particle numbers as obtained from the mean field only and those including the modes have different powers,  $-1.5$  and  $-0.67$  respectively. Already much earlier, around  $tm = 8000$ , this distribution starts to emerge, with 20% larger powers.

The power-law behaviour in the low momentum modes of the mean field apparently influences the quantum modes, in that their low momentum modes are enhanced in comparison to the classical  $T/\omega_k$ . We have seen this clearly in a plot of  $n_k\omega_k$  ( $\rightarrow T$  for classical thermal equilibrium) showing a peak at  $k = 0$  and a “classical plateau” at the interval  $k/m = 1.0 \dots 2.2$ . Similar behaviour has also been found in the other runs at  $\lambda/m^2 = 1/6$ ,  $E/Lm^2 = 2$  and  $\lambda/m^2 = 1/8$ ,  $E/Lm^2 = 4$ .

In a purely classical simulation using the same set of parameters power-law behaviour is *not* found. This suggests that the interaction of the mean field with the quantum modes plays a crucial role, even though the latter do not show power-law behaviour.

## 2. Time scales for energy exchange

In the previous section we obtained the scaling behaviour  $\propto \lambda^{-3}$  for the time scale of approximate equilibration based on the particle distribution. In this section we will use the energy density in the different parts of the field to find the short-time equilibration behaviour. Figs. 5-7 show the results from one of the simulations at  $\lambda/m^2 = 1/6$ ,  $E/Lm^2 = 4$ , plotted at different time scales. In Fig. 5, showing the early stage, the energy as

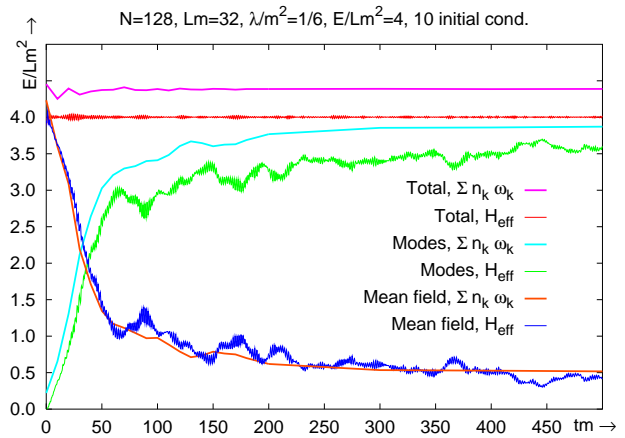


FIG. 5: Contributions to the energy density, for short times. From top to bottom at  $tm = 450$ :  $\sum_k n_k\omega_k$  (mean field + modes),  $E$  from  $H_{\text{eff}}$ ,  $\sum_k n_k\omega_k$  (modes only),  $E_{\text{modes}}$ ,  $\sum_k n_k\omega_k$  (mean field),  $E_{\text{mf}}$ .

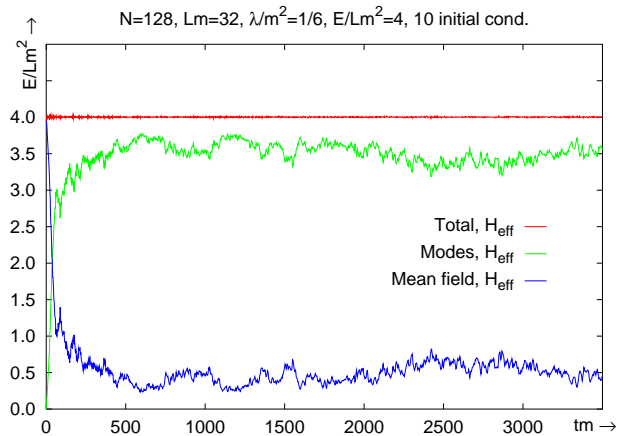


FIG. 6: Energy contributions for the same run as in Fig. 5 for intermediate times.

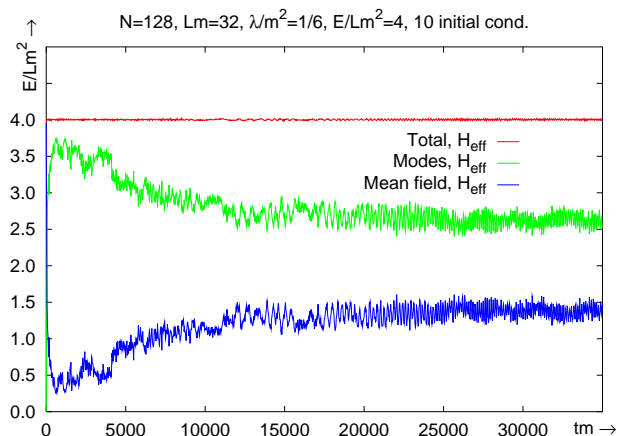


FIG. 7: As in Fig. 6 for long times.



obtained from the quasi-particles is also included. The quasi-particle picture appears to give a reasonable representation of the energies, with a roughly constant 10% mismatch in the total energy, to which we will come back, below. We furthermore see that the total energy in the quasi-particle picture is almost constant, corresponding to a quasi-particle number that is itself almost constant. This is consistent with the chemical potential found in the BE fits. We have checked that the dispersion relation of the quasi-particle energies is close to that of free particles,  $\omega_k = \sqrt{m_{\text{eff}}^2 + k^2}$ , but with an effective mass  $m_{\text{eff}}$  that is larger than  $m$ , as can be seen, for example, from the minimum values of  $\omega_k$  in Fig. 1, consistent with what follows from the effective potential. Coming back to the 10% mismatch in the quasi-particle energy: we have checked that it is neither a finite volume nor a finite lattice distance (spatial or temporal) effect. However, it does depend on the type of initial conditions used. For example a simulation with Bose-Einstein type initial conditions, as used in Ref. [3], with the same total energy, leads to a much smaller mismatch of almost 3%. It is important to note that we are looking at an effective description of an interacting theory and it is not expected that the total energy in these particles is completely equal to the actual total energy as derived from the effective Hamiltonian. One therefore expects them to be closer when interactions are less important. As we will indeed see in Section III B 2, at smaller coupling and energy the mismatch becomes much smaller.

Looking at the contributions  $E_{\text{mf}}$  and  $E_{\text{modes}}$  to  $H_{\text{eff}}$ , we see a relatively rapid transfer of energy from the mean field to the modes until a time of the order  $tm \approx 50$ . This exchange takes place fairly locally in momentum space, as is found by examining the mean field and mode contributions to  $n_k$ , a phenomenon that we call local  $k$ -space equilibration. At time  $tm \approx 100$  most of the particle number already comes from the modes, whereas the total distribution is still reasonably close to its initial form. After  $tm \approx 50$ , energy is still going to the modes, but with a slower rate. The behaviour in this second region, from  $tm \approx 50$  until  $tm \approx 2000$ , (see Fig. 6) can be fitted reasonably well with an exponential form

$$A + Be^{-t/\tau}, \quad (51)$$

yielding  $\tau m \approx 100 - 150$ . If we look at the long time behaviour, as plotted in Fig. 7, we see there is also a much longer time scale of the order 6000, on which energy is going back into the mean field. This time scale is comparable to the time scale of the emerging power-law behaviour, discussed in Section III A 1. The appearance of this power law is accompanied by a large increase in the particle number in the zero mode of the mean field and therefore also in the average energy density of the mean field. We recall that classical behaviour only becomes visible at larger time scales of the order 15000.

In order to make a quantitative comparison between different couplings and energies for the initial rapid exchange of energy between mean field and modes, related

$\tau m$	$E/Lm^2 = 1$	$E/Lm^2 = 2$	$E/Lm^2 = 4$
$\lambda/m^2 = 1/6$ ( $tm < 500$ )	137	70	39
$\lambda/m^2 = 1/8$ ( $tm < 800$ )	215	108	50
$\lambda/m^2 = 1/12$ ( $tm < 2500$ )	688	207	112

TABLE II: Initial energy-exchange time scales for the flat-ensemble initial conditions.

$\tau m$	Peak 1 & 2	Peak 1 & 3
“symmetric”, Hartree	$160 \pm 31$	$360 \pm 35$
“symmetric”, classical	$90 \pm 18$	$156 \pm 34$
“broken”, Hartree	$49 \pm 11$	$84 \pm 14$
“broken”, classical	$41 \pm 14$	$63 \pm 16$

TABLE III: Auto-correlation times for flat ensemble type initial conditions. In all cases the coupling  $\lambda/|\mu_{\text{ren}}^2| = 1/6$ . In the “symmetric phase”  $v^2 = 0$ ,  $\lambda/m^2 = 1/6$  and  $E/Lm^2 = 4$ , whereas in the “broken phase”  $v^2 = 6$ ,  $\lambda/m^2 = 1/12$ , and  $E/Lm^2 = 0.5$ .

to the local thermalization, we fitted the energy density in the mean field to a function of the form (51). The results are summarized in Table II. Using the energy in the quasi-particle picture, instead of the effective Hamiltonian, gives the same results.

Leaving out the run at the lowest coupling and energy,  $\lambda/m^2 = 1/12$ ,  $E/Lm^2 = 1$ , which we did not see thermalize, the time scale is roughly proportional to  $E^{-1}$  at constant coupling and to  $\lambda^{-3/2}$  at constant energy density:

$$\tau^{-1} \approx Cm(E/Lm^2)(\lambda/m^2)^{3/2}. \quad (52)$$

We have checked this behaviour explicitly by plotting the different energies as a function of  $(\lambda/m^2)^{3/2}(E/Lm^2)t$ , which led to  $C = 0.10$ .

For the lower energy density  $E/Lm^2 = 0.4$  the results are very similar to our simulation of the Gaussian wave packet, which we describe in Section III B. In particular, we encountered the local  $k$ -space equilibration. If we initially excite only a few modes this process can be seen even more clearly. We have not simulated long enough at this low energy density using the flat initial distribution to see the emergence of classical behaviour.

### 3. Auto-correlation time scales

To further investigate time scales, we also analysed the time-dependent auto-correlation function of the mean field, as in [10, 11]. Using flat ensemble initial conditions in both the “symmetric” and the “broken phase”, with either Hartree or classical dynamics the auto-correlation function was obtained from the average mean field only:

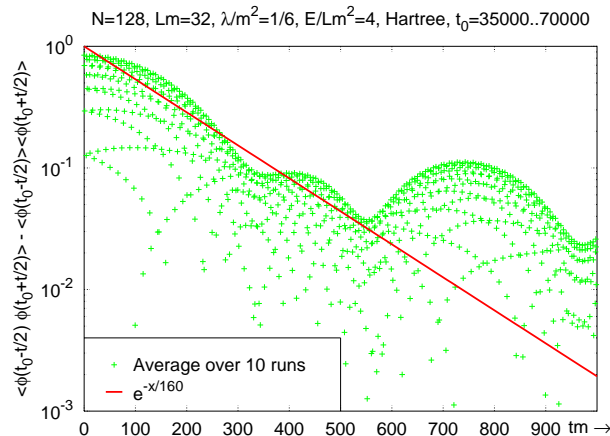


FIG. 8: Auto-correlation function for the average mean field using the flat Hartree ensemble. The lower “arcs” are an effect of sampling the oscillations  $\propto \log |\cos m_{\text{eff}} t|$  at discrete times.

$$C(t) = \overline{\langle \bar{\phi}(t_0 - t/2) \bar{\phi}(t_0 + t/2) \rangle}^{t_0} - \text{d.c.} \quad (53)$$

Here  $\bar{\phi}(t)$  denotes the spatially averaged mean field, the long overline includes averaging over a large time interval (which greatly reduces fluctuations), and d.c. stands for the disconnected piece. Fig. 8 shows an example in the large-time region, where the particle-number distribution has the behaviour shown in Fig. 4. The time average was taken over the region  $tm = 35000 \dots 70000$ , and ten initial configurations from the flat ensemble. We recall that the evident damping is seen also upon using only a single configuration [2], it is not caused by the average over initial conditions. The dip-like structure can be understood as being caused by interfering “twin peaks” in the spectral function [10]. The damping time is quantified using a “fit” of the form  $\exp(-t/\tau)$  through the first and second peaks. Using the third peak would give a roughly twice as large  $\tau$ . The results are given in Table III, where the errors are obtained with the jackknife method [12]. In the table a comparison is made with results from the classical approximation, and with results obtained in the “broken phase”.

In the “broken phase” there is hardly any difference between the classical and the Hartree results, although the Hartree result seems to indicate a slightly larger value. We recall that the particle distribution in this case approximates the Bose-Einstein form reasonably well, and furthermore, that the damping time is within a factor of two of the analytically computed value using perturbative quantum field theory in the two-loop approximation [2].

In the “symmetric phase” the Hartree result is roughly twice the classical value. It is hard to interpret this in any detail as the distribution function in the Hartree case is so “unconventional” (cf. Fig. 4) and also the classical case is far from thermalized. However, there

is a much more striking difference between the “broken” and “symmetric phase” results. At an 8 times larger energy, the auto-correlation time in the “symmetric phase” is not smaller, but instead larger by a factor of 3–4. One would expect qualitatively the opposite effect. For example, for a thermalized system at a temperature  $T$  the damping rate may be expected to scale, in the classical approximation, as  $(\lambda T)^{1/3}$ , and bluntly using the values  $\lambda T/m^3 = (1/6)(1/0.41)$  (“symmetric”, Table I) and  $(1/12) 1.1$  (“broken”, [2]) would give  $\tau_{\text{“symm”}}/\tau_{\text{“broken”}} = 0.62$  instead of the factor 3–4.

Comparing with the time scale for energy exchange, we see that at high energy density the damping time is 4–9 times larger than the energy-exchange time (cf. Table III and the upper-right entry in Table II). The systematics of this is unclear to us: at the lowest energy density (and smaller coupling) we find on the contrary that the damping time is about half the time scale for energy exchange (see also Sec. III B 3 for the Gaussian wave packet:  $\tau_{\text{damp}} \approx 3500$ ,  $\tau_{\text{exch}} \approx 7000$ ).

## B. Gaussian wave packet

In this section we focus on the initial condition specified by the Gaussian wave packet (9) with  $\lambda/m^2 = 0.1$ ,  $Am^2 = 2$  and  $\Phi = 2.60106$  (this value appeared in the preprint version of [5]), which gives an energy  $E/m^2 = 12.6$ . We used a volume  $Lm = 32$ , giving an energy density  $E/Lm^2 = 0.394$  which is practically equal to the smallest energy density 0.4 studied in the previous section with the flat ensemble. It is however still an order of magnitude larger than the highest energy densities studied in [5]. Our lattice size in this case was  $N = 256$  lattice points, and the temporal lattice distance  $a_0 = a/10$ , as before. We checked for finite volume and discretization effects by using different parameters and found that they do not influence the results discussed.

### 1. Particle distribution function

The initial Gaussian wave packet spreads and oscillates in the course of time and after  $t \gtrsim L/2$  the packet meets itself through the periodic volume. This can be seen from the plots of the mean field  $\phi(x)$ , see Fig. 1 in [5], which we have verified.

The initial wave packet (9) represents a pure state, which can still be analyzed in terms of particle numbers and frequencies obtained from the two-point functions, as in Eqs. (14). It is interesting to compare the so-obtained  $n_k$  with the coarse-grained particle distribution at later times. If we assume free-field evolution we can calculate  $n_k$  analytically, and it turns out that its average over (half) an oscillation period is time independent and close to the initial distribution, for large volumes. As derived in Appendix A this free-particle distribution for the Gaussian wave packet as initial condition is given by

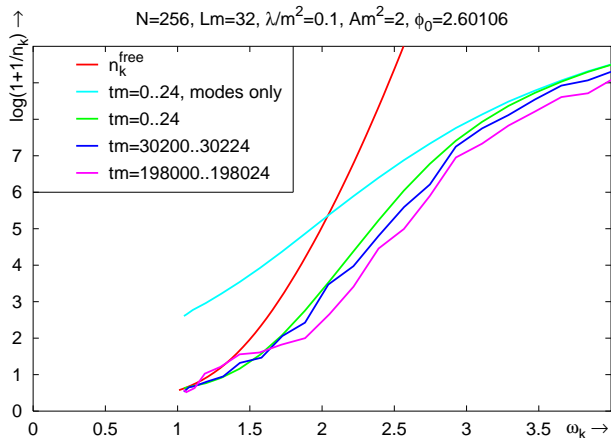


FIG. 9: Time development of particle number. The order in the key corresponds to the curves from top to bottom at  $\omega_k/m = 2.5$ .

$$n_k^{\text{free}} = \frac{\pi A \Phi^2 \sqrt{m^2 + k^2} e^{-k^2 A}}{L}. \quad (54)$$

In Fig. 9 we plot this free form together with the particle numbers obtained in a simulation.

We find it quite remarkable that already the earliest (time-averaged) distribution deviates significantly from the initial form (54). A closer look shows that this deviation originates entirely from the first period ( $tm = 0 \dots 2\pi$ ). After that short time the distribution is almost stationary. Only after a time  $tm = \mathcal{O}(10^5)$  do we see deviations arise. However, in the mean time there is an extensive exchange of energy between the modes and the mean field: initially all particle number and energy is contained in the mean field, while in the later stage it is just the opposite.

After  $tm \approx 30000 - 40000$  classical behaviour, i.e.  $n_k \rightarrow T/\omega_k$ , starts to emerge: the lower-momentum modes become under-occupied, while the higher modes become over-occupied. At no stage does the distribution resemble the Bose-Einstein form (50). We recall that also with the flat ensemble we did not see quantum thermalization at similarly low energy densities.

Bettencourt et al. [5] studied the power spectrum of the subtracted two-point function  $S_k(t) - S_k(0)$  at times  $tm \lesssim 200$ . This appeared to show power behaviour  $\sim k^{-3}$  to  $k^{-4}$ , which was interpreted as evidence for the absence of BE-like thermalization. As mentioned above we also see no BE thermalization at this low energy density, but we find that the power behaviour is not without ambiguities. The aim of the subtraction in  $S_k(t) - S_k(0)$  was to eliminate the vacuum contribution  $1/(2\sqrt{m^2 + k^2})$  from  $S_k$ . At large  $k$  this is a rather delicate procedure. For instance, a quasi-particle behaviour  $S_k(t) = (n_k(t) + 1/2)/\sqrt{m(t)^2 + k^2}$  with a thermal-like mass  $m(t)$  that is expected to be larger than  $m$  in the

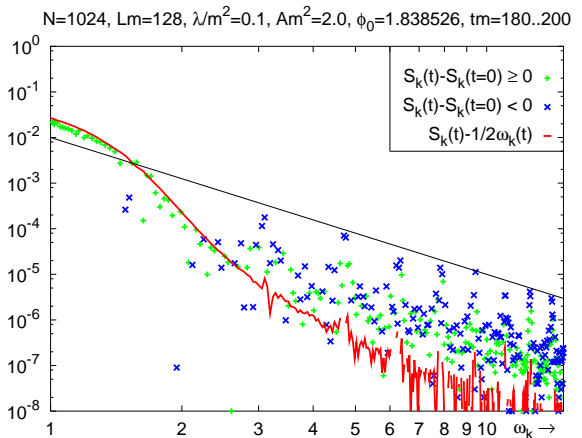


FIG. 10: The power spectrum  $S_k(t) - S_k(0)$  and  $n_k(t) - 1/2\omega_k(t) = S_k(t) - 1/2\omega_k(t)$  for  $tm = 180 \dots 200$ . The line represents a power  $\propto \omega^{-3}$  touching the negative values of  $S_k(t) - S_k(0)$ .

“symmetric phase”, would give a negative result at large  $k$ ,  $S_k(t) - S_k(0) \approx -[m(t)^2 - m^2]/4k^3$ , where we neglected an assumed exponentially small  $n_k(t)$ .

We would like to stress here the good features of the observables  $n_k$  and  $\omega_k$  defined in Eqs. (14). In Fig. 10 we have plotted  $S_k(t) - 1/2\omega_k(t) = n_k(t)/2\omega_k(t)$ , as well as  $S_k(t) - S_k(0)$ , for the same parameters ( $\Phi = 1.838526$ ,  $Am^2 = 2$ ,  $Lm = 128$ ,  $N = 1024$ ) and in the same time regime as used in [5]. (We averaged over  $tm = 180 - 200$ , which hardly affects  $n_k(t)/2\omega_k(t)$  as it is practically constant.) The plot of  $S_k(t) - S_k(0)$  looks very similar to the ones shown in [5]. There is a lot of scatter at large  $\omega_k$  ( $\approx k$ ) and a more detailed analysis shows negative values interspersed with positive values (indicated separately for the power spectrum). On the other hand  $n_k/2\omega_k$  shows less scatter and is mostly positive (only for  $\omega_k > 4$  do negative values occur). However, note that the larger  $\omega$  region could be affected by lattice artefacts.

## 2. Energy densities and time scales

To get an estimate of the time scales involved we compare the energy densities in the mean field, in the modes and in the total field for the Gaussian wave packet initial condition, as we did in Sec. III A 2 for the flat ensemble at higher energy densities. For short times these are plotted in Fig. 11, together with the energy as derived from the quasi-particle picture (17). For long times they are plotted in Fig. 12.

We see that the quasi-particle representation of the energies is in this case extremely good, there is hardly any visible difference with the exact energies based on  $H_{\text{eff}}$ .

Furthermore, for early times (Fig. 11) there is an oscillatory behaviour with a period  $tm \approx 130$ . Note that, due

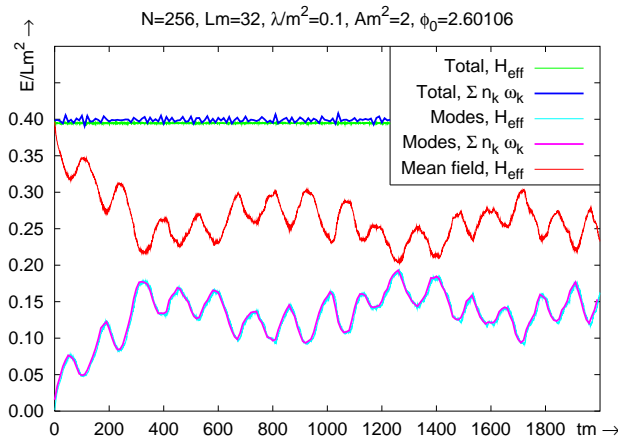


FIG. 11: The different energies for the Gaussian wave packet initial conditions at short times. From top to bottom: energy from modes and mean field, energy from mean field, energy from modes.

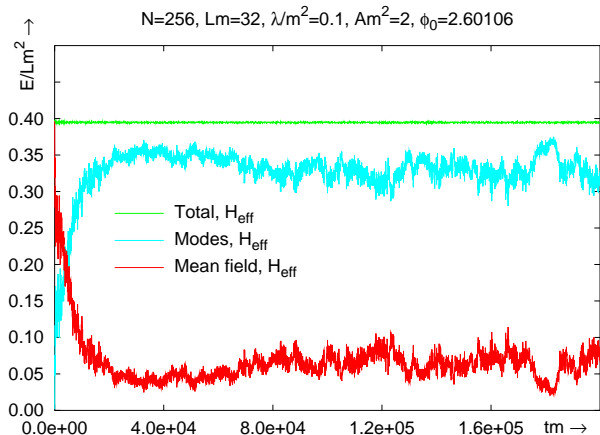


FIG. 12: The different energies for the Gaussian wave packet initial conditions at long times.

to the periodic boundary conditions on the system with size  $Lm = 32$ , the Gaussian packet already “meets itself” after a time  $tm = 16$ , much shorter than this resonance time. The resonance is caused by the difference between the effective mass terms of the modes and mean field,  $\approx 2\lambda\phi^2$ . This mass difference has a small value, fluctuating around  $0.030 - 0.050$ , corresponding to a period  $210 - 126$ , approximately the observed period.

The rate at which energy flows to the modes can be seen at long times (Fig. 12). The energy in the mean field in the interval  $tm < 60000$  can be fitted reasonably well to an exponential function of the form (51), yielding an equilibration time scale  $\tau m \approx 7000$ , roughly two orders of magnitude larger than what was found in the “broken phase” at similar energy densities and couplings.

Using a sum of waves as initial condition at similar energy density shows the same kind of resonance in the energy exchange between mean field and modes, with

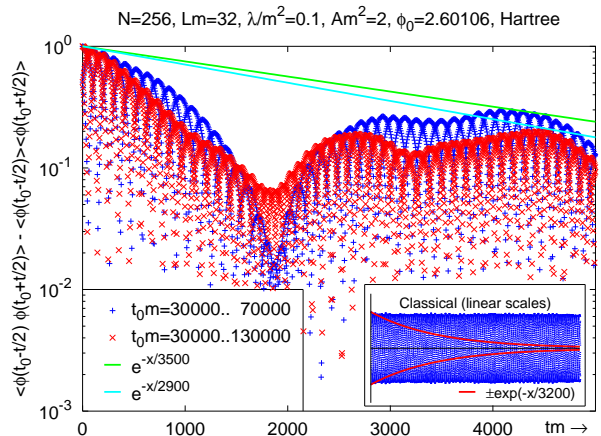


FIG. 13: The auto-correlation function as determined from the average mean field only. The result when using classical dynamics is shown in the insert on a linear scale, with an exponential fit to the Hartree result.

period  $\approx 170$  and mass difference fluctuating around  $0.02 - 0.04$ . Averaging over the flat ensemble the oscillations die out after  $tm \approx 4000 - 5000$ .

### 3. Time scales from the auto-correlation function

We also evaluated the auto-correlation function for the Gaussian wave packet. Since we do not average over initial conditions we cannot calculate a statistical error. We therefore averaged over two different time intervals, giving some idea of the size of the statistical uncertainty. The result is plotted in Fig. 13. At this low energy, the damping time is roughly half the energy equilibration time. The inset shows – on a linear scale – the result for classical dynamics, using identical initial conditions. The exponential curve is a fit to the Hartree result: classically there is no visible damping.

It would be interesting to compare the result with the flat initial ensemble at the same energy density. However, for these low energies we need to simulate for very long times, which is quite a numerical effort. We therefore only calculated the auto-correlation times for the faster evolving high energy runs discussed in Section III A.

## IV. SCATTERING

In this section we will discuss scattering features of the Hartree approximation. First we take a fresh look at the possibility of scattering via inhomogeneous mean fields by considering an initial state of two localized particle wave packets in position space. Next we give a perturbative explanation of “local  $k$ -space equilibration”, our numerical result that the modes appear to equilibrate with the mean field primarily when they have the same wave

number. This occurs especially at low energy density and weak coupling and it has the effect that the initial particle distribution in the mean field is taken over approximately by the modes. We end this section with a brief discussion of higher-order scattering and thermalization.

### A. Scattering of two wave packets

For homogeneous mean fields the Hartree approximation cannot describe true scattering in which the momenta of the particles in the initial and final states differ. However, in the inhomogeneous case the particles can truly scatter off the mean field. It is interesting to take an intuitive look at this in position space. Consider an initial two-particle state described by wave packets  $\psi_{1,2}$ :

$$|\psi_1\psi_2\rangle = \hat{b}^\dagger[\psi_1]\hat{b}^\dagger[\psi_2]|0\rangle, \quad \hat{b}^\dagger[\psi] = \sum_{\mathbf{k}} \psi_{\mathbf{k}} \hat{b}_{\mathbf{k}}^\dagger. \quad (55)$$

This is a non-Gaussian and pure state, for which

$$C_{\text{ren}}(\mathbf{x}, t; \mathbf{x}, t) = |\psi_1(\mathbf{x}, t)|^2 + |\psi_2(\mathbf{x}, t)|^2 \quad (56)$$

where

$$\psi(\mathbf{x}, t) = \sum_{\mathbf{k}} \psi_{\mathbf{k}}^* f_{\mathbf{k}}(\mathbf{x}, t). \quad (57)$$

Linearizing the Hartree equations in the “broken phase”, writing  $\phi = v + \phi'$  and keeping terms linear in  $\phi'$  while treating  $|\psi|^2$  as being of the same order as  $\phi'$ , gives

$$\begin{aligned} (\partial_t^2 - \Delta + m^2)\phi' &= -3\lambda (|\psi_1|^2 + |\psi_2|^2), \\ (\partial_t^2 - \Delta + m^2 + 6\lambda v\phi')\psi_{1,2} &= 0. \end{aligned} \quad (58)$$

If the wave packets approach each other within a distance of order  $1/m$  they will scatter.

So the interaction of the quantum modes with the classical modes of the inhomogeneous mean field does lead to indirect scattering. Note that this happens especially in the “broken phase”: in the “symmetric phase”  $v = 0$  and the backreaction of the mean field disturbance  $\phi'$  to the particle waves  $\psi_{1,2}$  is suppressed.

### B. Local $k$ -space equilibration

To give an analytic interpretation of the “local  $k$ -space equilibration” it is useful to focus on various interaction terms in the effective Hamiltonian (16). Although derived from a quantum system, this Hamiltonian can also be seen as describing interacting classical fields  $\phi$  and  $f_\alpha$ . It will be convenient to split the modes  $f_\alpha$  in a free part and a perturbation:

$$f_\alpha(x, t) = f_\alpha^0(x, t) + g_\alpha(x, t), \quad (59a)$$

$$f_\alpha^0(x, t) = \frac{e^{ik_\alpha x - i\omega_\alpha t}}{\sqrt{2\omega_\alpha L}}, \quad (59b)$$

with  $\omega_\alpha^2 = m^2 + k_\alpha^2$ .  $f_\alpha^0$  will then play the role of an external field, as it is not altered by the interaction.

We will show in the following that for not too large coupling and energy the equation of motion for  $g_\alpha$  reduces to that of a driven harmonic oscillator. Making use of the corresponding scattering diagrams we then conclude that, approximately, the only momentum modes of  $g_\alpha$  that are excited are those also present in the mean field. Since we will focus on the initial behaviour, when the system is still far from equilibrium and there is not yet a temperature, we will only use zero-temperature perturbation theory.

We can write out the effective Hamiltonian in terms of the classical fields  $\phi$ ,  $g_\alpha$  and the “external field”  $f_\alpha^0$ . In the “symmetric phase” and to second order in  $g_\alpha$ , this leads to the following interaction terms and corresponding vertex factors

$$\frac{1}{4}\lambda\phi^4 \quad 6\lambda \quad (60a)$$

$$3\lambda\phi^2 \sum_{\alpha} \Re(f_\alpha^0 g_\alpha^*) \quad 3\lambda \quad (60b)$$

$$\frac{3}{2}\lambda\phi^2 \sum_{\alpha} |g_\alpha|^2 \quad 3\lambda \quad (60c)$$

$$6\lambda \sum_{\alpha, \beta} \Re(f_\alpha^0 g_\alpha^*) \Re(f_\beta^0 g_\beta^*) \quad 3\lambda \quad (60d)$$

whereas in the “broken phase”, writing  $\phi = v + \phi'$ , we also have the three-point interactions

$$\lambda v \phi'^3 \quad 6\lambda v \quad (61a)$$

$$6\lambda v \phi' \sum_{\alpha} \Re(f_\alpha^0 g_\alpha^*) \quad 3\lambda v \quad (61b)$$

$$3\lambda v \phi' \sum_{\alpha} |g_\alpha|^2 \quad 3\lambda v \quad (61c)$$

In a first approximation we neglect the back reaction on the mean field and assume it is just oscillating around its minimum as a superposition of waves:

$$\phi(x, 0) = \sum_{i=1}^{i_{\text{max}}} A_i \sin(\omega_{K_i} t) \cos(K_i x - \psi_i) \quad (62)$$

where  $\psi_i$  are random phases and  $\omega_{K_i} = \sqrt{m^2 + K_i^2}$ .

The exact Hartree dynamical equation for the mode perturbation  $g_\alpha(x)$  in terms of its Fourier transform  $g_{\alpha k}$  is given by

$$\begin{aligned} (\partial_t^2 + \omega_k^2)g_{\alpha k} &= -3\lambda \int dx (\phi(x))^2 + C_{\text{ren}}(x) \\ &\times \left( \frac{e^{i(k_\alpha - k)x - i\omega_\alpha t}}{\sqrt{2\omega_\alpha}} + \frac{1}{L} \sum_{k'} e^{i(k' - k)x} g_{\alpha k'} \right). \end{aligned} \quad (63)$$

Neglecting for the moment the higher order terms containing  $C_{\text{ren}}$  and  $g_{\alpha k}$  in the integral, the  $x$  integration

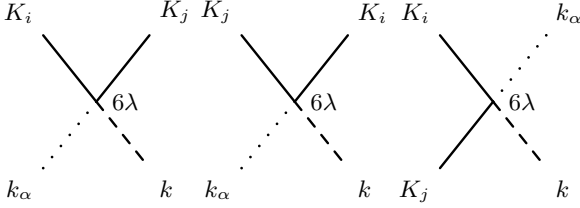


FIG. 14: Tree level scattering diagrams involving a single perturbation mode  $g_\alpha$ . Solid lines denote  $\phi$ , a dotted line  $f_\alpha^0$ , and the dashed line denotes  $g_\alpha$ . Time runs from left to right.

can be performed, resulting in a sum over plane waves. The equation is that of a driven harmonic oscillator

$$(\partial_t^2 + \omega_k^2)g_{\alpha k}(t) = \sum_j B_j e^{-i\Omega_j t}, \quad (64)$$

which leads to resonances that grow linearly in time for  $\omega_k^2 = \Omega_j^2$ . By inserting the explicit form (62) into Eq. (63) we find for each pair  $K_i, K_j$  four different resonance relations:

$$\omega_k = \pm\omega_\alpha \pm \omega_{K_i} \pm \omega_{K_j}, \quad (65)$$

(with uncorrelated  $\pm$ ), while the  $x$  integration gives four different momentum relations:

$$k = k_\alpha + \eta_1 K_i + \eta_2 K_j, \quad (66)$$

where  $\eta_{1,2} = \pm 1$ .

These two relations describe energy-momentum conservation in scattering processes involving a single 4-point vertex, the interaction (60b). Only  $2 \rightarrow 2$  processes involving this vertex can conserve energy and momentum. Furthermore, in  $1+1$  dimensions (since all particles have the same mass) it follows that the pair of incoming momenta must be equal to the pair of outgoing momenta. From the energy relation (65) it then follows that there are three possible diagrams, drawn in Fig. 14, creating a  $g_\alpha$  particle with momentum  $k$ . The momentum relation (66) now gives us three possibilities,

$$k = \eta_2 K_j \quad k_\alpha = -\eta_1 K_i \quad (67a)$$

$$k = \eta_1 K_i \quad k_\alpha = -\eta_2 K_j \quad (67b)$$

$$k = k_\alpha \quad \eta_1 K_i = -\eta_2 K_j \quad (67c)$$

For the last possibility  $k = k_\alpha$ , the  $\phi(x)^2$  term contributes a constant. These terms only give rise to a time-dependent mass shift between the modes and mean field. We can conclude that to leading order the only excited modes are given by

$$g_{\pm K_i, \pm K_j}. \quad (68)$$

Note that only when just one mean field mode is excited (i.e. when  $i_{\max} = 1$ ) the modes will remain diagonal.

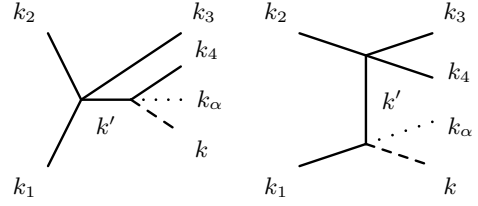


FIG. 15: Leading  $2 \rightarrow 4$  scattering diagrams creating a  $g_\alpha^k$  particle in the “symmetric phase”. The intermediate line represents the retarded Green function.

We will now look at the neglected terms. The renormalized mode sum  $C_{\text{ren}}(x)$  is equal to

$$C_{\text{ren}}(x) = \sum_\alpha \left( f_\alpha^{0*}(x)g_\alpha(x) + f_\alpha^0(x)g_\alpha^*(x) + |g_\alpha(x)|^2 \right). \quad (69)$$

As we just showed, in lowest order,  $g_\alpha$  is only non-zero for  $k_\alpha \in \{K_i\}$  and therefore the only non-zero Fourier components of  $C_{\text{ren}}(x)$  are the same as those in  $\phi(x)^2$ :  $k = \pm K_i \pm K_j$ . Therefore including the first order result for  $C_{\text{ren}}(x)$  in Eq. (63) will not change the set of excited modes. Finally, including the last term in Eq. (63) using the first order result (68) we can also find its contribution. The  $x$  integration gives a  $\delta_{k', k \pm K_i \pm K_j}$ . The frequencies of the correction to  $g_\alpha$  are therefore of the form  $\omega_{k \pm K_i \pm K_j}$  and we find exactly the same relation as following from Eqs. (65) and (66).

The above treatment can be extended by making a systematic expansion in  $\lambda$ ,  $\phi = \phi_0 + \lambda\phi_1 + \lambda^2\phi_2 + \dots$ ,  $f_\alpha = f_\alpha^0 + \lambda f_\alpha^1 + \lambda^2 f_\alpha^2 + \dots$ , and using Green function techniques along the lines of [13].

As a check we performed a simulation, exciting only two modes  $K_1$  and  $K_2$  at low energy ( $E/Lm^2 = 0.04$ ) and small coupling ( $\lambda/m^2 = 1/12$ ). The assumption of a free oscillating mean field turned out to be extremely good. We also checked the explicit form of one of the modes by examining  $|f_{K_1}|^2$ . We expect  $f$  to contain the two Fourier modes  $K_1$  and  $K_2$ , and therefore  $|f|^2$  to contain momenta  $2K_1, 2K_2, K_1 + K_2$  and  $K_1 - K_2$ , which were indeed the only modes found. In similar simulations at higher energy we found that the back reaction to  $\phi$  became more important, but the set of excited modes remained the same.

### C. Higher order scattering

In order for the system to thermalize it is necessary that particles can change their momenta by scattering. As mentioned above,  $2 \rightarrow 2$  scattering cannot change the initial momenta in  $1+1$  dimensions. (With re-summed off shell propagators this restriction does not apply, cf. the nontrivial spectral functions in [10] and [14], and the thermalization found in [4].) Therefore at least one extra vertex is needed. In the “symmetric phase” only four-point vertices exist, as in Eqs. (60). The interaction (60b) is leading over (60c) and (60d), because it is first order in  $g_\alpha$ , and since initially all energy is in the mean field, the

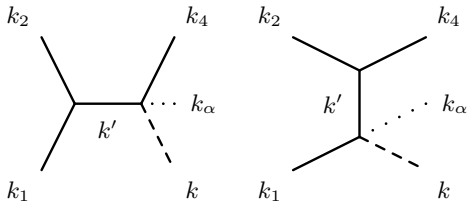


FIG. 16: Leading  $2 \rightarrow 3$  scattering diagrams creating a  $g_\alpha^k$  particle in the “broken phase”.

leading contribution to  $g$ -particle production comes from the two diagrams in Fig. 15.

At this point it is interesting to realize what happens if the mean field is homogeneous. In that case  $g_\alpha$  always carries momentum  $k_\alpha$ . For inhomogeneous systems this restriction is lifted and thermalization becomes possible.

In the “broken phase” both the couplings (60) and (61) contribute and there are three- and four-point interactions. The leading contribution to  $g$ -particle production in this case comes from the two diagrams in Fig. 16. Intuitively one expects the finite range of the interaction in the “broken phase”, due to off-shell particle exchange, to lead to more efficient thermalization than the zero range interaction in the “symmetric phase”. This is indeed what we observed.

## V. DISCUSSION

We will start this discussion with a summary of the behaviour at high and low energy density. This appears to be the distinguishing criterion for the thermalization behaviour of the Hartree approximation for inhomogeneous systems, rather than, for example, an initial state being pure, as for the Gaussian wave packet, or mixed, as for the flat ensemble.

At high energy density  $E/Lm^2 \gg 1$  we see that the distribution  $n_k$  acquires features of a thermal quantum, i.e. Bose-Einstein distribution. There is a time- and coupling-dependent chemical potential, of order unity in mass units. The temperature is roughly proportional to  $\sqrt{E/L}$  and independent of the coupling. The coupling determines the time scale on which the approximate thermalization becomes visible. The initial rapid exchange of energy between modes and mean field occurs on a time scale described by Eq. (52). The quasi-particle picture is reasonable and the total particle number is very constant, in correspondence with the chemical potential. However, there is a mismatch between the total energy as derived from the effective Hamiltonian and that obtained from the quasi-particles, Eqs. (16) and (17). As we already pointed out, this mismatch depends on the initial conditions, for example a Bose-Einstein type initial conditions cf. Ref. [3] leads to a much smaller mismatch. For an interacting theory it is not expected that a quasi particle picture based on free particles would give precisely the same value as what follows from effective Hamiltonian and indeed the mismatch was practically invisible at

lower energy and coupling. Furthermore, a considerable amount of the total energy comes from the zero mode, about 10%, making it very sensitive to the precise particle distribution and probably making deviations from the quasi-particle picture more pronounced.

After a very long time the energy flows back into the mean field, accompanied by the emergence of a power-law distribution for  $n_k$  as a function of momentum  $k$ . Such power-law behaviour has not been found in the “broken phase”, and also classical simulations do not show such a behaviour, indicating that the back reaction of the modes plays an essential role. It is interesting to note that Boyanovsky et al. [15] also found power-law behaviour for the occupation numbers, although it is unclear if the same mechanism is behind their finding. In their study of a  $3 + 1$  dimensional  $O(N)$  model in the large  $N$  approximation, the power-law is caused by a nonlinear resonance of the back reaction of the modes on themselves, with terms of the form  $1/(\omega_k - m)$ , diverging as  $1/k^2$  in the limit  $k \rightarrow 0$ . This would give a  $1/k^4$  behaviour for the particle number, different from what is found here. Furthermore, we only find power-law behaviour in the total- and mean-field-particle numbers, but not in that of the modes. The difference in power and the absence of power-law behaviour in the modes makes it improbable that the physical mechanism behind the resonances is the same.

At low energy density  $E/Lm^2 \ll 1$ , for the flat ensemble as well as for the pure-state wave packet, we do not find approximate thermalization to a BE distribution. Instead, the form of the total distribution  $n_k$  remains the same for times that are many tens of thousands in units of  $m^{-1}$ . The distribution then slowly turns over into a classical distribution. However, there is still an extensive exchange of energy between the mean field and the modes, leading to what we call local  $k$ -space equilibration, for which we were able to find an interpretation based on a perturbative calculation. At low energy, the time scale for this process is much longer than would follow from Eq. (52), found at high energy densities. Furthermore, at short times the energy densities in the mean field and modes separately show a remarkable oscillatory behaviour, not seen at higher energies, which is caused by a difference in the effective mass of the mean field and modes.

We obtained several time scales: for approximate Bose-Einstein thermalization, for the early-time exchange of energy between mean field and modes, for the auto-correlation function and for the evolution to a classical distribution. Most of these are much longer in the “symmetric phase” than in the “broken phase”, due to the absence of the finite range interaction.

According to [3], the BE-thermalization-time scale in the “broken phase” is of the order  $25 - 35$  for  $E/Lm^2 = 0.5$ , while here, in the “symmetric phase”,  $m\tau_{\text{BE}} = 1500 - 1600$  for  $E/Lm^2 = 4$  (both at  $\lambda/|\mu_{\text{ren}}^2| = 1/6$ ).

The energy-exchange time scale in the “broken phase” gives a result that is close to  $\tau_{\text{BE}}$ , whereas in the “sym-

metric phase” it is related to local  $k$ -space equilibration, much shorter than  $\tau_{\text{BE}}$ , and it shows the behaviour (52). For  $E/Lm^2 = 0.5$  and  $\lambda/|\mu_{\text{ren}}^2| = 1/6$ , Eq. (52) gives  $\tau m \approx 300$ , much longer than the 25–40 we found in the “broken phase” at the same energy and coupling.

Also the damping time, obtained from auto-correlation functions, is much longer than in the “broken phase”, even at much higher energy and larger coupling. Compared to the value obtained using classical dynamics, it is roughly twice as large. In the “broken phase”, both values are comparable in size. At low energies the damping time seems to be much longer, but this needs more study.

The last time scale is that of classical equilibration. Since we are just solving a large number ( $2N^2 + 1$ ) of local classical non-linear equations, one may expect classical equipartition to set in at some point. This equipartition is, however, non-trivial because of the large number of conserved charges [2]. For example, the emerging classical temperature is of order  $E/N$  and not  $E/N^2$  [2].<sup>3</sup> Depending on energy and coupling we can already see a first emergence of classicality at times  $\tau m = \mathcal{O}(10^4)$ . This is still about an order of magnitude longer than what was found in the “broken phase” in [3]. However, full classical equilibrium is expected only for huge times, much larger than the  $\tau m = \mathcal{O}(10^6)$  found in the “broken phase” for an artificially small system at  $E/Lm^2 = 36$  [2], and beyond the already large times of order  $10^5$  reached in this study.

Remarkably, the equilibration time scale found in [1] using classical dynamics appears to be *shorter*. The empirical formula [1]

$$1/m\tau_{\text{class}} = 5.8 \cdot 10^{-6} (6\lambda T/m^3)^{1.39}, \quad (70)$$

with  $T = E/N$  the classical equilibrium temperature, would give equilibration times  $tm = \mathcal{O}(10^5) - \mathcal{O}(10^7)$  for the various parameters used here. This difference in time scales can be interpreted as follows. Classical dynamics has also been studied in the Hartree approximation, and the latter shows up as an unstable fixed point of the full dynamics [1]. This Hartree fixed point depends on the initial conditions. In our case the mode functions are initialized with quantum-vacuum form (5), and the resulting dynamics (seen as a classical system with order  $N^2$  fields) appears to linger for a very long time near a Hartree fixed point, longer than when using classical dynamics.

For our inhomogeneous initial conditions we have not been able to pin down the fixed point analytically, but intuitively one may expect the system to be close to it when the mean field has lost most of its energy and has started fluctuating about a homogeneous average. Making a homogeneous approximation to this situation would lead

to a Hartree stationary state. Such a state can have an arbitrary particle distribution  $n_k$ , which, given our out-of-equilibrium initial conditions, turns out to have BE features when the energy density  $E/Lm^2 \gg 1$ . Apparently, when the energy density is small,  $E/Lm^2 \ll 1$ , the system leaves the fixed-point region before BE-like thermalization sets in, because we have seen only classical-like equilibration emerging in this case.

Finally, we comment on the results of Bettencourt et al. [5]. As mentioned in Sec. III B 1, we have essentially confirmed their numerical results. The energy density in the simulations in [5] was rather low, namely  $E/Lm^2 = 0.00042$  and  $0.0045$ , so in view of our results summarized above, no sign of a BE distribution is to be expected with the Hartree approximation at the times  $tm \lesssim 200$  covered in [5], nor at any time later.

It is remarkable that we do find Bose-Einstein behaviour at larger energies  $E/Lm^2 \gg 1$ , but of course, the fact remains that one needs to improve on the Hartree approximation in order to achieve thermalization at all energies. This may take huge times at low energy densities.

It has been remarked [5] that the Hartree approximation is expected to be valid up to times  $tm \sim m^2/\lambda = \mathcal{O}(10)$ . We agree with this statement when applied to the detailed time-evolution of observables, but it does not necessarily apply to observables such as our quasi-particle distribution  $n_k(t)$  or energy  $\omega_k(t)$ , which are coarse grained in time and space and/or averaged over initial conditions in the Hartree ensemble approximation. For comparison, consider a gas of classical point particles with Lennard-Jones interactions. Any numerical approximation to the detailed time evolution will soon go dismally wrong due to the chaotic nature of the system, but this does not preclude an accurate evaluation of, say, a coarse-grained particle-distribution function. With this in mind we have studied our system for times as large as seemed necessary, which led to very large times indeed. First experience [16] indicates that the situation is not very different in 3+1 dimensions, where also large equilibration times may be expected for the  $\phi^4$  model at moderate couplings and energy densities.

## Acknowledgments

We thank Jeroen Vink for his collaboration in the initial stages of this work. We thank Gert Aarts, Anders Tranberg and Michele Simionato for useful discussions. This research was supported by FOM/NWO.

## APPENDIX A: PARTICLE NUMBER OF THE GAUSSIAN WAVE PACKET

We calculate here the initial two-point functions for the Gaussian wave packet initial condition (9), the corresponding particle number  $n_k$  and energy  $\omega_k$ , and their

<sup>3</sup> For  $N$  spatial lattice sites there are  $2N^2$  real degrees of freedom in the mode functions.



subsequent free field expressions. The calculations will be made in the continuum limit, in our finite periodic volume.

The mean field contributions to the two-point functions are given by

$$S(x, y)^{\text{mf}} = \overline{\phi(x)\phi(y)} - \overline{\phi(x)} \overline{\phi(y)}, \quad (\text{A1a})$$

$$U(x, y)^{\text{mf}} = \overline{\pi(x)\pi(y)} - \overline{\pi(x)} \overline{\pi(y)}, \quad (\text{A1b})$$

where at first we shall average only over space, i.e.

$$\overline{\phi(x)\phi(y)} = \frac{1}{L} \int_0^L dz \phi(x+z)\phi(y+z). \quad (\text{A2})$$

The initial mean field is given by Eq. (9), or in terms of its Fourier transform:

$$\phi_k = \int dx e^{-ikx} \phi(x) = \Phi \sqrt{2\pi A} e^{-k^2 A/2}. \quad (\text{A3})$$

Since  $\pi(0) = 0$ , the free-field (i.e. for  $\lambda \rightarrow 0$  and  $\mu \rightarrow \mu_{\text{ren}} = m$ ) evolution of  $\phi_k$  is given by:

$$\phi_k(t) = \phi_k(0) \cos(\omega_k^{(0)} t), \quad (\text{A4})$$

where  $\omega_k^{(0)} = \sqrt{m^2 + k^2}$ . A straightforward calculation gives

$$S_k^{\text{mf}} = \left(1 - \delta_{k,0}\right) \frac{\phi_k^2 \cos^2(\omega_k^{(0)} t)}{L}, \quad (\text{A5a})$$

$$U_k^{\text{mf}} = \left(1 - \delta_{k,0}\right) \frac{(\omega_k^{(0)})^2 \phi_k^2 \sin^2(\omega_k^{(0)} t)}{L}, \quad (\text{A5b})$$

where the delta functions come from the disconnected pieces. The modes just contribute the vacuum fluctuations:

$$S_k^{\text{modes}} = \frac{1}{2\omega_k^{(0)}}, \quad U_k^{\text{modes}} = \frac{\omega_k^{(0)}}{2}. \quad (\text{A6})$$

Adding the contributions in Eqs. (A5) and (A6) and applying the definition (14), the initial instantaneous particle number and frequency become

$$n_k(0) = \frac{1}{2} \left( \sqrt{2\omega_k^{(0)} \phi_k^2 / L + 1} - 1 \right), \quad (\text{A7a})$$

$$\omega_k(0) = \frac{\omega_k^{(0)}}{\sqrt{2\omega_k^{(0)} \phi_k^2 / L + 1}}. \quad (\text{A7b})$$

Using free field dynamics the instantaneous particle number would get an oscillating component according to Eqs. (A5). If we also course grain in time, the disconnected parts of  $S$  and  $U$  vanish, while both  $\cos^2$  and  $\sin^2 \rightarrow 1/2$ . We then find

$$n_k^{\text{free}} = \frac{\omega_k^{(0)} \phi_k^2}{2L}, \quad \omega_k^{\text{free}} = \omega_k^{(0)}, \quad (\text{A8})$$

which are time independent.

For large volumes  $2\omega_k^{(0)} \phi_k^2 / L \ll 1$ , expressions (A7a) and (A7b) reduce to (A8). For the parameters as used in Section III,  $A = 2$ ,  $\Phi = 2.60106$ ,  $Lm = 32$ , we have

$$\frac{2\omega_k^{(0)} \phi_k^2}{L} \approx 5.3 \sqrt{1 + k^2/m^2} e^{-2k^2/m^2}. \quad (\text{A9})$$

Plotting  $n_k(0)$  (or  $\log(1 + 1/n_k(0))$ ) versus  $\omega_k(0)$  we find that this only compares well with a similar plot of  $n_k^{\text{free}}$  versus  $\omega_k^{\text{free}}$  for  $k \gtrsim 2m$ . So at times  $tm \gg 1$  it is best to use the time-averaged free-field determinations for the comparison with the interacting Hartree evolution.

- 
- [1] G. Aarts, G. F. Bonini, and C. Wetterich, Phys. Rev. **D63**, 025012 (2001), hep-ph/0007357.
- [2] M. Sallé, J. Smit, and J. C. Vink, Phys. Rev. **D64**, 025016 (2001), hep-ph/0012346.
- [3] M. Sallé, J. Smit, and J. C. Vink, Nucl. Phys. **B625**, 495 (2002), hep-ph/0012362.
- [4] J. Berges and J. Cox, Phys. Lett. **B517**, 369 (2001), hep-ph/0006160.
- [5] L. M. A. Bettencourt, K. Pao, and J. G. Sanderson, Phys. Rev. **D65**, 025015 (2002), hep-ph/0104210.
- [6] F. Cooper, S. Habib, Y. Kluger, and E. Mottola, Phys. Rev. **D55**, 6471 (1997), hep-ph/9610345.
- [7] D. Boyanovsky, H. J. de Vega, R. Holman, and J. F. J. Salgado, Phys. Rev. **D54**, 7570 (1996), hep-ph/9608205.
- [8] G. Aarts and J. Smit, Nucl. Phys. **B555**, 355 (1999), hep-ph/9812413.
- [9] J. Smit, *Introduction to Quantum Fields on a Lattice* (Cambridge University Press, Cambridge, UK, 2002).
- [10] M. Sallé, J. Smit, and J. C. Vink, in *Strong and electroweak matter 2000 - Proceedings of the SEWM2000 Meeting*, edited by C. P. Korthals Altes (World Scientific, Singapore, 2000), hep-ph/0008122.
- [11] M. Sallé, J. Smit, and J. C. Vink, Nucl. Phys. Proc. Suppl. **94**, 427 (2001), hep-lat/0010054.
- [12] R. G. Miller, Biometrika **61**, 1 (1974).
- [13] G. Aarts and J. Smit, Phys. Lett. **B393**, 395 (1997), hep-ph/9610415.
- [14] G. Aarts and J. Berges, Phys. Rev. **D64**, 105010 (2001), hep-ph/0103049.
- [15] D. Boyanovsky, C. Destri, H. J. de Vega, R. Holman, and J. F. J. Salgado, Phys. Rev. **D57**, 7388 (1998), hep-ph/9711384.
- [16] J. C. Vink, private communication.